A Typha Angustifolia-like MoS_2/carbon nanofiber composite for high performance Li-S batteries

Xingxing Gu,[1,2]* Han Kang[1], Chengbin Shao,[1] Xiaolei Ren[1], Xiaoteng Liu[1,2]*

[1] Chongqing Key Laboratory of Catalysis and New Environmental Materials, College of Environment and Resources, Chongqing Technology and Business University, Chongqing 400067, China

[2] Department of Mechanical and Construction Engineering, Faculty of Engineering and Environment, Northumbria University, Newcastle upon Tyne NE1 8ST, UK

*for correspondences: x.gu@ctbu.edu.cn; terence.liu@northumbria.ac.uk

A Typha Angustifolia-like MoS_2/carbon nanofiber composite as both the chemically trapping agent and redox conversion catalyst for lithium polysulfides have been successfully synthesized via a simple hydrothermal method. By applying the Typha Angustifolia-like MoS_2/carbon nanofiber as the interlayer for pure sulfur cathode, the cycling performance and coulombic efficiency have been improved significantly, which the capacity degradation is only 0.09% per cycle and the coulombic efficiency can reach as high as 99%.

Keyword: Li-S batteries, MoS_2/BCF, electrocatalysis, chemically trapping, polysulfides

INTRODUCTION

Lithium-sulfur (Li-S) batteries attracted considerable interests due to its high energy density (2600 Wh/kg) as well as the cathode material, sulfur, is cost-effective, natural abundant, and environment friendly(Gu and Lai, 2019). However, Li-S batteries are plagued with various challenges. Among those, the serious lithium polysulfides (LiPSs) shuttling, inducing large capacity degradation, severe polarization, sluggish reaction kinetics and inefficient self-discharge, is one of the most significant issues(Liu et al., 2019;Xu et al., 2019).

In view of such a serious situation, tremendous efforts have been made to suppress polysulfides shutting through physical confinements and chemical adsorption by construction various kinds of nanostructures, such as the nonpolar porous carbon(Rehman et al., 2016;Guo et al., 2018), graphene(Yin et al., 2016), carbon nanotubes (Yang et al., 2018), as well as the polar metal oxides(Gu et al., 2016;Song et al., 2018), metal sulfides(He et al., 2019;Lin et al., 2019), metal carbide(Chen et al., 2018;Dong et al., 2018;Song et al., 2019), metal nitride(Jiao et al., 2019;Wang et al., 2019), etc. Accordingly, the LiPSs shuttling has alleviated to some extent. While recently, researchers focused on the electrocatalysis of reducing sulfur to LiPSs and oxidizing Li_2S_2/Li_2S to LiPSs even to sulfur during the charge-discharge process, which is important for achieving high reversible capacity and coulombic efficiency.

By applying the electrocatalysis concept of enhancing the redox reactions of polysulfides, increasing numbers of catalysts suitable for redox conversion of lithium polysulfides have been reported(Jeong et al., 2017;Liu et al., 2018;Hao et al., 2019;He et al., 2019;Jiao et al., 2019;Lin et al., 2019;Yuan et al., 2019).

In this work, we synthesized a new 1D nanostructure, Typha Angustifolia-like MoS_2/carbon nanofiber composite as both the chemical trapping agent and redox conversion catalyst for LiPSs to enhance the sulfur cathode performances. The sulfur cathode with the MoS_2/carbon nanofiber interlayer illustrate an initial capacity as high as 926.1 mAh/g at charge-discharge current of 0.5 C, even after 300 cycles, a reversible capacity of 661.5 mAh/g could maintain.

EXPERIMENTAL

Materials Preparation

Bamboo carbon fiber (BCF) preparation: the bamboo stick was immersed in 8M KOH solution and hydrothermal reaction for 12 h. Then the resulted bamboo fiber was dried and annealed at 800 °C for 2 h under Ar atmosphere. Finally, the BCF was obtained by washing with distilled water and drying overnight.

BCF/MoS_2 preparation: 114 mg Ammonium molybdate tetrahydrate ($(NH_4)_6Mo_7O_{24}•4H_2O$) and stoichiometric overdose thiourea were dissolved in 60 mL distilled water, then 40 mg BCF dispersed in the

mixture solution by ultrosonication. Next the solution was transferred into the Teflon autoclave and reacted for 12 h at 200 °C. At that time, a black composite was obtained. After washing by the distilled water and ethanol and drying, the composite was annealed in H_2/N_2 (5% volume percent of H_2) atmosphere at 800 °C for 1 h to obtain the finally Typha Angustifolia-like BCF/MoS_2 composites.

Materials Characterizations

The samples' structures were characterized by X-ray diffraction (XRD, (Model LabX-6000, Shimadzu, Japan) and JSM-7001F scanning electron microscope (SEM) (JEOL, Japan).

Electrochemical Measurements

S, carbon black and polyvinylidene fluoride (analytical reagent, Sigma-Aldrich) in a weight ratio of 80:10:10, were mixed with solvent of 1-methyl-2-pyrrolidinone (analytical reagent, Sigma-Aldrich). After stirring for 12h, the electrode slurry was obtained. Then the slurry was pasted on the Aluminium foil via the blade-coating method. After drying at 60 °C in a vacuum oven overnight, the electrode was cut into wafers with a size of 0.5 cm^2 and a weight of approximately 1.5 mg. The interlayer was made by BCF/MoS_2, carbon black and polytetrafluoroethylene in a weight ratio of 80:10:10 with solvent of 1-methyl-2-pyrrolidinone to form a flexible film. After drying at 60 °C in a vacuum oven overnight, the film was cut into wafers with a diameter of

11 mm, thickness of 150 μm and a weight of approximately 1.2 mg.

Then batteries were assembled in a glove box (Vigor, China), using the lithium metal as the counter electrode, polypropylene (Celgard 2300) as the separator, and 1 M lithium bis(trifluoromethane)sulfonimide (LiTFSI) in 1,3-dioxolane/1,2-dimethoxyethane (DOL/DME) (1:1, v/v) containing 0.2 M $LiNO_3$ as the electrolyte. And the BCF/MoS_2 wafer could be placed between the separator and the electrode as the interlayer during the battery assembling process. Finally, the charge and discharge performances of the coin cells were tested with a LAND CT-2001A instrument (Wuhan, China) and the cyclic voltammetry (CV) curves were performed on a CHI 660D electrochemical workstation (CHI Instrument, Shanghai, China), both which the potential range was controlled between 1.5 and 3.0 V at room temperature. And the capacities were calculated based on the sulfur mass. Additionally, the electrode impedance spectrums (EIS) were tested on CHI 660E (frequency range from 100 kHz and 10 mHz).

RESULTS AND DISCUSSIONS

Firstly, the XRD was used to examine crystallization structure of the synthesized product. As shown in Figure 1, The BCF/MoS_2 has been successfully synthesized by using a simple hydrothermal method. From the XRD spectrum of BCF, there is a wide peak around at 2 theta of 23°, which belongs to the partial graphitization of carbon, implying the good

conductivity of BCF(Gu et al., 2015). While from the spectrum of BCF/MoS_2, the peak belonging to the graphitization carbon has been covered by other strong peaks. All these peaks could be ascribed to the MoS_2, and the crystal phase could match well with the MoS_2 stand PDF card (37-1492).

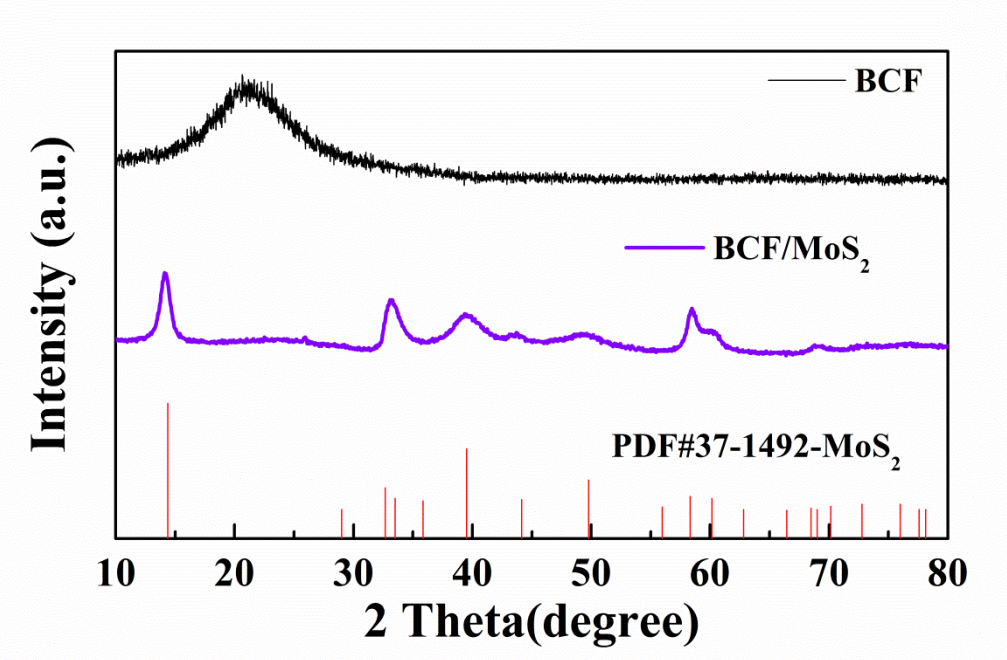

Figure 1 XRD spectra of BCF, BCF/MoS_2 and Stand XRD spectrum of MoS_2.

Following the morphology information of BCF and BCF/MoS_2 have been investigated by SEM. As shown in Figure 2a, the bamboo carbon with unique fiber structure has successfully synthesized. While in Figure 2b and 2c, the BCF as a core, and the MoS_2 grown in the direction of the nanofiber line as a shell has been observed. Such a unique one-dimensional structure is very much like Typha Angustifolia as shown in Figure 2d.

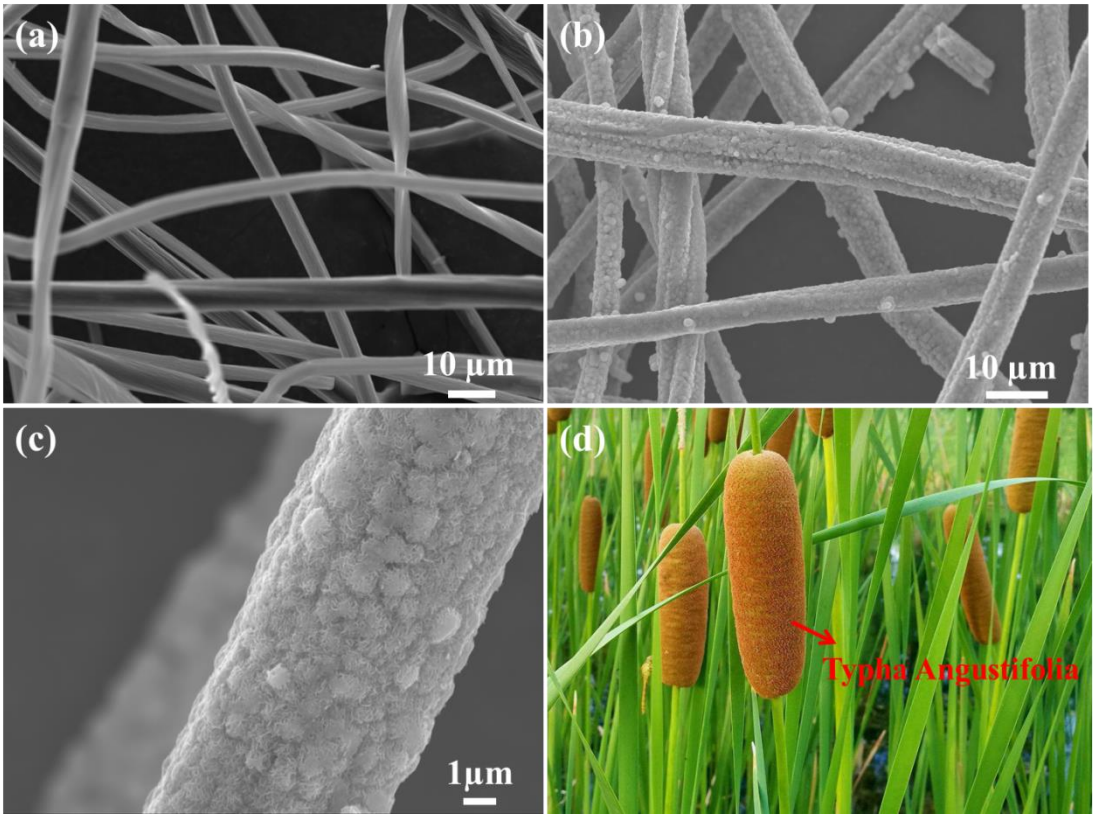

Figure 2 SEM images of (a) bamboo carbon fiber, (b-c) BCF/MoS_2 and (d) the digital photo of Typha Angustifolia.

Then the electrochemical performances of the sulfur cathode with and without the BCF/MoS_2 interlayer have been investigated. As shown in Figure 3a, there are two obvious and stable redox peaks for the sulfur cathode with BCF/MoS_2 interlayer. While in Figure 3b, pure sulfur electrode (BCF/MoS_2 interlayer) illustrate deformed and widened redox peaks in the CV curves, which suggests a sluggish kinetic process(Li et al., 2017;Liu et al., 2018). Comparing the peak potentials (Figure 3c) during the redox reactions, it is evident that the sulfur cathode with BCF/MoS_2 interlayer shows higher reduction potential and lower oxidation potential than that without BCF/MoS_2 interlayer, indicating that the BCF/MoS_2 interlayer significantly lowers the electrode

polarization(Gu et al., 2015;Wang et al., 2018;He et al., 2019). This can be attributed to the catalysis effect of MoS_2 on the oxidation/reduction of lithium polysulfides/Li_2S(Wang et al., 2018;He et al., 2019). In terms of the onset potentials shown in Figure 3d, the onset potential of the sulfur cathode with BCF/MoS_2 interlayer in the oxidation reaction is ≈2.23 V, compared with ≈2.21 V for the pure sulfur cathode without BCF/MoS_2 interlayer. With respect to the reduction reaction, the onset potentials for sulfur cathode with BCF/MoS_2 interlayer are ≈2.42 and ≈2.12 V, compared with ≈2.4 and ≈2.1 V for the pure sulfur cathode without BCF/MoS_2 interlayer, which are lower by ≈20 mV. These results demonstrate that by inserting a conductive BCF/MoS_2 interlayer, the redox kinetics are accelerated and the polarization losses are also significantly reduced for the Li-S battery.(Gu et al., 2015;Li et al., 2017;He et al., 2019)

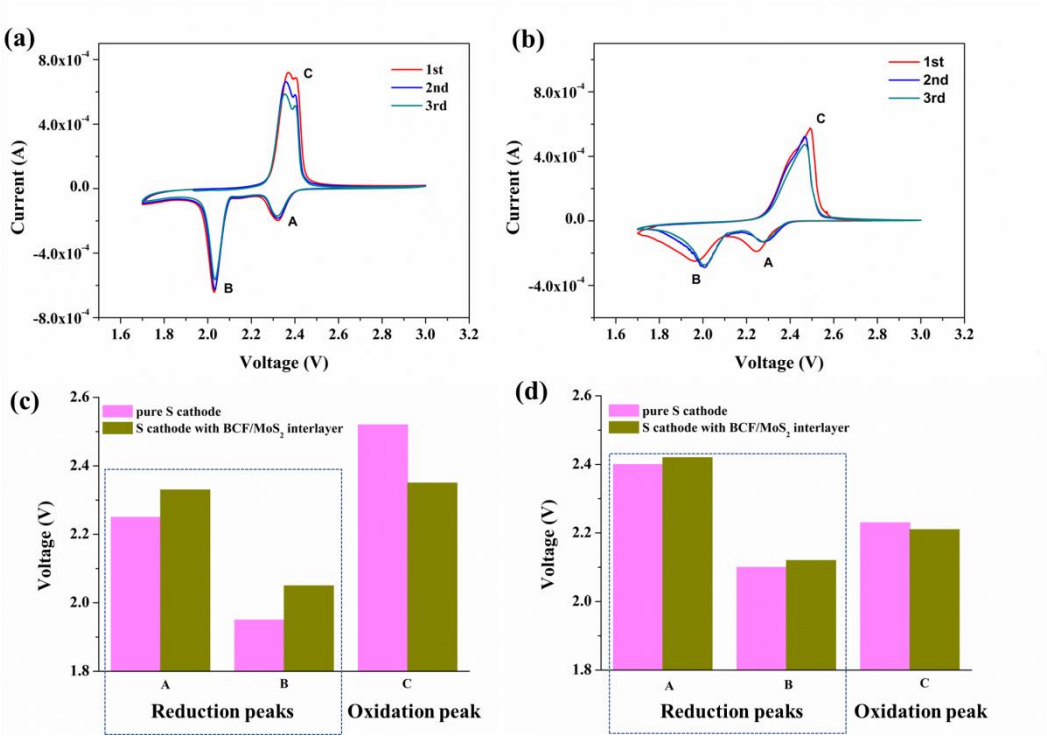

Figure 3 Kinetics of electrochemical reactions in Li-S batteries. CV test of (a) sulfur cathode with BCF/MoS_2 interlayer and (b) pure sulfur electrode. Corresponding (c) peak potentials and (d) onset potentials of the sulfur cathodes with and without BCF/MoS_2 interlayer from the first CV cycle in (a) and (b).

Finally, we carried out the long cycling performances and rate capabilities of the sulfur cathode with and without BCF/MoS_2 interlayer. As shown in Figure 4a, the sulfur cathode with interlayer shows a high initial specific capacity of 926.1 mAh/g. After cycling 300 cycles, it can still maintain a high reversible capacity of 661.5 mAh/g, and the capacity degradation rate is only 0.09% per cycle. However, the pure sulfur cathode without BCF/MoS_2 interlayer, only demonstrates an initial capacity of 510 mAh/g and extremely low reversible capacity of 56.3 mAh/g after 300 cycles. By contrast, the initial average discharge capacity of the pure sulfur cathode without interlayer is ≈400 mAh/g

lower than the sulfur cathode with BCF/MoS_2 interlayer, indicating significant dissolution and loss of LiPSs into the electrolyte during the initial cycles, and such severe dissolution and loss continues throughout the whole charge and discharge process because the ultimate reversible capacity is also extremely low. Additionally, from figure 4b, it is clearly observed that the sulfur cathode with BCF/MoS_2 interlayer shows far better rate capabilities compared to the one without BCF/MoS_2 interlayer. Even the charge-discharge current increases to 2 C, a reversible capacity of around 456 mAh/g could still be reserved, and after the current switch to low density of 0.2 C, a recoverable capacity of approximately 900 mAh/g could reach. Therefore, the BCF/MoS_2 is highly effective as polysulfide immobilizers to enhance the cycling life and rate capabilities(Gu et al., 2015).

What's more, it can be observed that the sulfur cathode with BCF/MoS_2 interlayer demonstrate an excellent coulombic efficiency approximately 99%, but the sulfur cathode without interlayer shows an obvious weaker coulombic efficiency, particularly in the tens of cycles ahead. The coulombic efficiency results indicates that BCF/MoS_2 as electrocatalyst could significantly accelerate the redox reaction in Li-S batteries and improve the coulombic efficiency(Gu et al., 2015;Jeong et al., 2017;Wang et al., 2018).

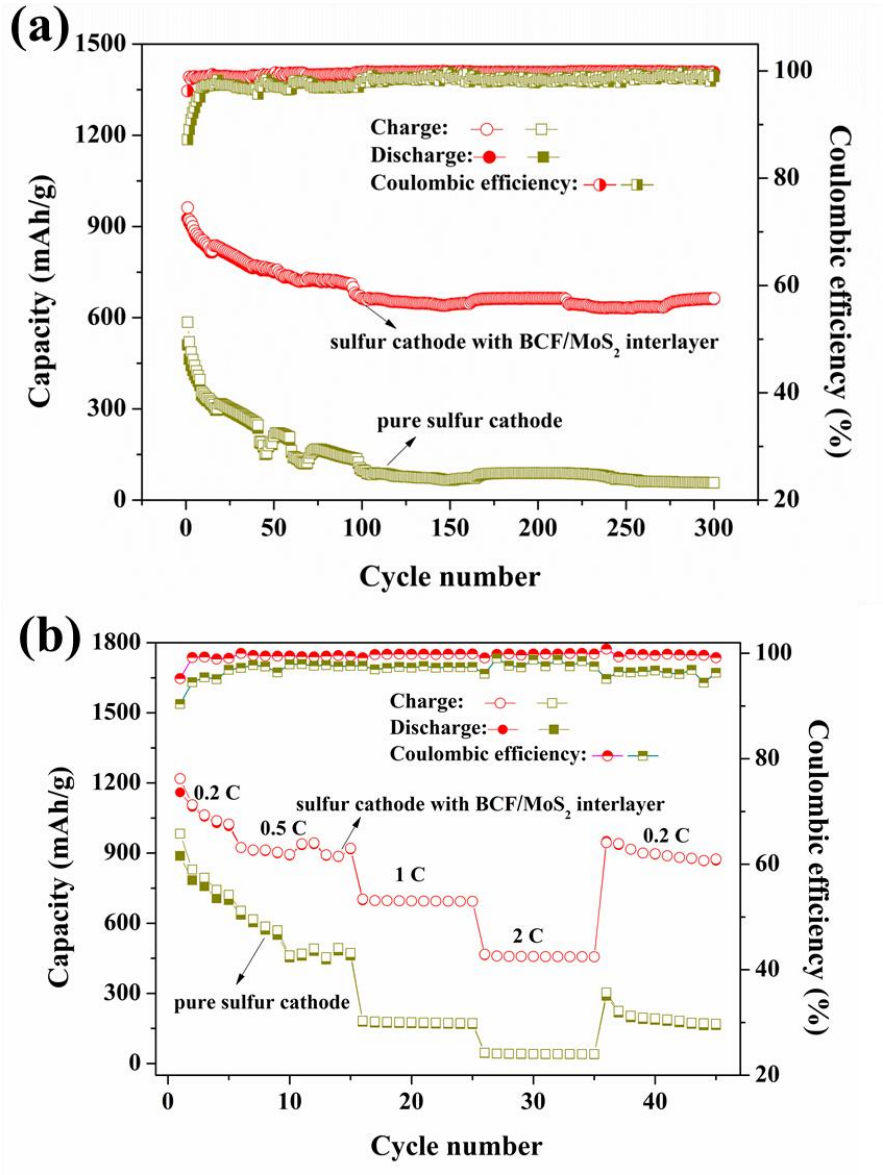

Figure 4 (a) The long-cycling performances of sulfur cathode with and without BCF/MoS_2 interlayer at charge-discharge current of 0.5 C, (b) the rate capabilities of sulfur cathode with and without BCF/MoS_2 interlayer.

CONCLUSIONS

In summary, the Typha Angustifolia-like MoS_2/carbon nanofiber composites has been successfully employed as the interlayer in Li–S batteries. The BCF/MoS_2 interlayer bestows Li–S batteries excellent long-term cycle stability (only 0.09% capacity fade per cycle) and high

coulombic efficiency (99%) even when the sulfur content is as high as 65% in the electrode. The exceptional performance can be attributed to (i) the resultant conductive fiber networks, providing conductive skeletons for the electrons transfer; (ii) abundant gaps and pores to store the sulfur; (iii) polar MoS_2 shell chemically trapping the LiPSs as well as catalyzing the LiPSs redox reaction. Therefore, the unique Typha Angustifolia-like MoS_2/carbon nanofiber interlayer has shed a light for high-performance Li-S batteries development.

AUTHOR CONTRIBUTIONS

All authors listed have made a substantial, direct and intellectual contribution to the work, and approved it for publication.

ACKNOWLEDGEMENT

This work was supported by the National Natural Science Foundation of China (No. 51902036), Natural Science Foundation of Chongqing Science & Technology Commission (No. cstc2019jcyj-msxm1407), Natural Science Foundation of Chongqing Technology and Business University (No. 1952009), the Venture & Innovation Support Program for Chongqing Overseas Returnees (Grant No. CX2018129), the Science and Technology Research Program of Chongqing Municipal Education Commission (Grant No. KJQN201900826 and KJQN201800808), Innovation Group of New Technologies for Industrial Pollution Control of Chongqing Education Commission (Grant No. CXQT19023), Open

Research Fund of Chongqing Key Laboratory of Catalysis and New Environmental Materials (Grant No. KFJJ2018082), and the Engineering and Physical Sciences Research Council (EPSRC) (Grant No. EP/S032886/1).

ORCID

Xingxing Gu https://orcid.org/0000-0002-5145-7751

REFERENCES

Chen, G., Song, X., Wang, S., Chen, X., and Wang, H. (2018). Two-dimensional molybdenum nitride nanosheets modified Celgard separator with multifunction for Li-S batteries. *J. Power Sources* 408**,** 58-64. doi:10.1016/j.jpowsour.2018.10.078

Dong, Y., Zheng, S., Qin, J., Zhao, X., Shi, H., Wang, X., Chen, J., and Wu, Z.-S. (2018). All-MXene-based integrated electrode constructed by Ti_3C_2 nanoribbon framework host and nanosheet interlayer for high-energy-density Li–S batteries. *ACS Nano* 12**,** 2381-2388. doi:10.1021/acsnano.7b07672

Gu, X., and Lai, C. (2019). One dimensional nanostructures contribute better Li–S and Li–Se batteries: Progress, challenges and perspectives. *Energy Stor. Materi.* 23**,** 190-224. doi:10.1016/j.ensm.2019.05.013

Gu, X., Lai, C., Liu, F., Yang, W., Hou, Y., and Zhang, S. (2015). A conductive interwoven bamboo carbon fiber membrane for Li–S batteries. *J. Mater. Chem. A* 3**,** 9502-9509. doi:10.1039/c5ta00681c

Gu, X., Tong, C.J., Wen, B., Liu, L.M., Lai, C., and Zhang, S. (2016). Ball-milling synthesis of ZnO@sulphur/carbon nanotubes and $Ni(OH)_2$@sulphur/carbon nanotubes composites for high-performance lithium-sulphur batteries. *Electrochim. Acta* 196**,** 369-376. doi:10.1016/j.electacta.2016.03.018

Guo, Y., Jiang, A., Tao, Z., Yang, Z., Zeng, Y., and Xiao, J. (2018). High-performance lithium-sulfur batteries with an IPA/AC modified separator. *Front. Chem.* 6**,**

222. doi:10.3389/fchem.2018.00222

Hao, B., Li, H., Lv, W., Zhang, Y., Niu, S., Qi, Q., Xiao, S., Li, J., Kang, F., and Yang, Q.H. (2019). Reviving catalytic activity of nitrides by the doping of the inert surface layer to promote polysulfide conversion in lithium-sulfur batteries. *Nano Energy* 60**,** 305-311. doi:10.1016/j.nanoen.2019.03.064

He, J., Hartmann, G., Lee, M., Hwang, G.S., Chen, Y., and Manthiram, A. (2019). Freestanding 1T MoS_2/graphene heterostructures as a highly efficient electrocatalyst for lithium polysulfides in Li–S batteries. *Energy Environ. Sci.* 12**,** 344-350. doi:10.1039/c8ee03252a

Jeong, T.G., Choi, D.S., Song, H., Choi, J., Park, S.-A., Oh, S.H., Kim, H., Jung, Y., and Kim, Y. T. (2017). Heterogeneous catalysis for lithium–sulfur batteries: enhanced rate performance by promoting polysulfide fragmentations. *ACS Energy Lett.* 2**,** 327-333. doi:10.1021/acsenergylett.6b00603

Jiao, L., Zhang, C., Geng, C., Wu, S., Li, H., Lv, W., Tao, Y., Chen, Z., Zhou, G., Li, J., Ling, G., Wan, Y., and Yang, Q.H. (2019). Capture and catalytic conversion of polysulfides by in situ built TiO_2-MXene heterostructures for lithium–sulfur batteries. *Adv. Energy Mater.* 9**,** 1900219. doi:10.1002/aenm.201900219

Li, L., Chen, L., Mukherjee, S., Gao, J., Sun, H., Liu, Z., Ma, X., Gupta, T., Singh, C.V., Ren, W., Cheng, H.M., and Koratkar, N. (2017). Phosphorene as a polysulfide immobilizer and catalyst in high-performance lithium-sulfur batteries. *Adv. Mater.* 29**,** 1602734. doi:10.1002/adma.201602734

Lin, H., Zhang, S., Zhang, T., Cao, S., Ye, H., Yao, Q., Zheng, G.W., and Lee, J.Y. (2019). A cathode-integrated sulfur-deficient Co_9S_8 catalytic interlayer for the reutilization of "lost" polysulfides in lithium-sulfur batteries. *ACS Nano* 13**,** 7073-7082. doi:10.1021/acsnano.9b02374

Liu, D., Zhang, C., Zhou, G., Lv, W., Ling, G., Zhi, L., and Yang, Q.H. (2018). Catalytic effects in lithium-sulfur batteries: promoted sulfur transformation and reduced shuttle effect. *Adv. Sci.* 5**,** 1700270. doi:10.1002/advs.201700270

Liu, Y., Kou, W., Li, X., Huang, C., Shui, R., and He, G. (2019). Constructing patch-Ni-shelled Pt@Ni nanoparticles within confined nanoreactors for

catalytic oxidation of insoluble polysulfides in Li-S batteries. *Small* 15**,** e1902431. doi:10.1002/smll.201902431

Rehman, S., Gu, X., Khan, K., Mahmood, N., Yang, W., Huang, X., Guo, S., and Hou, Y. (2016). 3D vertically aligned and interconnected porous carbon nanosheets as sulfur immobilizers for high performance lithium-sulfur batteries. *Adv. Energy Mater.* 6**,** 1502518. doi:10.1002/aenm.201502518

Song, X., Wang, S., Chen, G., Gao, T., Bao, Y., Ding, L.-X., and Wang, H. (2018). Fe-N-doped carbon nanofiber and graphene modified separator for lithium-sulfur batteries. *Chem. Eng. J* 333**,** 564-571. doi:10.1016/j.cej.2017.09.186

Song, Y., Zhao, S., Chen, Y., Cai, J., Li, J., Yang, Q., Sun, J., and Liu, Z. (2019). Enhanced sulfur redox and polysulfide regulation via porous VN-modified separator for Li-S batteries. *ACS Appl. Mater. Interf.* 11**,** 5687-5694. doi:10.1021/acsami.8b22014

Wang, M., Fan, L., Tian, D., Wu, X., Qiu, Y., Zhao, C., Guan, B., Wang, Y., Zhang, N., and Sun, K. (2018). Rational design of hierarchical SnO_2/1T-MoS_2 nanoarray electrode for ultralong-life Li–S batteries. *ACS Energy Lett.* 3**,** 1627-1633. doi:10.1021/acsenergylett.8b00856

Wang, Y., Zhang, R., Pang, Y.C., Chen, X., Lang, J., Xu, J., Xiao, C., Li, H., Xi, K., and Ding, S. (2019). Carbon@titanium nitride dual shell nanospheres as multi-functional hosts for lithium sulfur batteries. *Energy Stor. Mater.* 16**,** 228-235. doi:10.1016/j.ensm.2018.05.019

Xu, L., Zhao, H., Sun, M., Huang, B., Wang, J., Xia, J., Li, N., Yin, D., Luo, M., Luo, F., Du, Y., and Yan, C. (2019). Oxygen vacancies on layered niobic acid that weaken the catalytic conversion of polysulfides in lithium-sulfur batteries. *Angew Chem. Int. Ed. Engl.* 58**,** 11491-11496. doi:10.1002/anie.201905852

Yang, G., Tan, J., Jin, H., Kim, Y.H., Yang, X., Son, D.H., Ahn, S., Zhou, H., and Yu, C. (2018). Creating effective nanoreactors on carbon nanotubes with mechanochemical treatments for high-areal-capacity sulfur cathodes and lithium anodes. *Adv. Funct. Mater.***,** 1800595-1800603.

doi:10.1002/adfm.201800595

Yin, L.-C., Liang, J., Zhou, G.-M., Li, F., Saito, R., and Cheng, H.M. (2016). Understanding the interactions between lithium polysulfides and N-doped graphene using density functional theory calculations. *Nano Energy* 25**,** 203-210. doi:10.1016/j.nanoen.2016.04.053

Yuan, H., Peng, H.J., Li, B.Q., Xie, J., Kong, L., Zhao, M., Chen, X., Huang, J.Q., and Zhang, Q. (2019). Conductive and catalytic triple-phase interfaces enabling uniform nucleation in high-rate lithium-sulfur batteries. *Adv. Energy Mater.* 9**,** 1802768. doi:10.1002/aenm.201802768

Yuan, H., Peng, H.-J., Li, B.-Q., Xie, J., Kong, L., Zhao, M., Chen, X., Huang, J.-Q., and Zhang, Q. (2019). Conductive and catalytic triple-phase interfaces enabling uniform nucleation in high-rate lithium-sulfur batteries. *Adv. Energy Mater.* 9**,** 1802768. doi:10.1002/aenm.201802768